DOI: 10.1002/ejic.200800514

The Role of Axial Ligation in Nitrate Reductase: A Model Study by DFT Calculations on the Mechanism of Nitrate Reduction

Kuntal Pal[a] and Sabyasachi Sarkar*[a]

Keywords: Density functional calculations / Enzyme models / Oxidoreductases / Molybdenum

The reactivity differences of the model anionic complexes $[Mo(mnt)_2(X)(PPh_3)]^-$ [mnt^{2-} = 1,2-dicyanoethylenedithiolate; X = SPh (**1a**), SEt (**1b**), Cl (**1c**), Br (**1b**)] towards oxygen atom transfer from nitrate, which is a key step performed by nitrate reductase, has been investigated by density functional theory calculations. Unlike complexes **1a** and **1b**, complexes **1c** and **1d** do not react with nitrate. Thermodynamically, all these complexes have a similar ability to generate the pentacoordinate active state $[Mo(mnt)_2(X)]^-$ by dissociation of PPh_3, although the inaccessibility of the d_{xy} orbital in **1c**,**d** and the instability of the corresponding nitrate-bound enzyme substrate (ES) type complex contributes to their failure to reduce nitrate. The nature of the ES complex for **1a**,**b** is described. The variation in the experimental data due to the change of axial ligation from SPh to SEt on the catalytic pathway has also been addressed. The gas-phase and solvent-corrected potential energy surface for the reaction of **1a**,**b** with nitrate are established with fully optimized minima and transition states.

Introduction

A large number of mononuclear molybdoenzymes (and tungstoenzymes)[1] contain a molybdenum (or tungsten) atom coordinated to an organic cofactor classically known as molybdopterin (MPT) and presently as pyranopterindithiolene.[2] These enzymes mainly catalyze important redox reactions that maintain the global carbon, sulfur and nitrogen cycles. An oxygen (atom) transfer reaction (OAT),[3] where the oxygen atom is ultimately derived from, or incorporated into, water to or from a substrate in a two-electron redox reaction, dominates in these redox reactions. According to Hille's classification,[4] the majority of molybdoenzymes can be classified into three families represented by xanthine oxidase (XO),[5] sulfite oxidase (SO)[6] and DMSO reductase.[7] This classification closely follows the composition of molybdopterin at the metal centers and the catalytic activity. Nitrate reductase,[7,8] which belongs to the DMSO reductase family, plays an important role in respiration, where it catalyzes the reduction of nitrate to nitrite via an OAT reaction [Equation (1)].

$$NO_3^- + 2\,H^+ + 2\,e^- \rightleftharpoons NO_3^- + H_2 \quad (1)$$

Several synthetic (deoxo)Mo^{IV} complexes[9] with dithiolene chelating ligands have been reported as proposed models of the active site of nitrate reductase. However, these models do not show a functional property similar to the OAT reaction (Scheme 1).

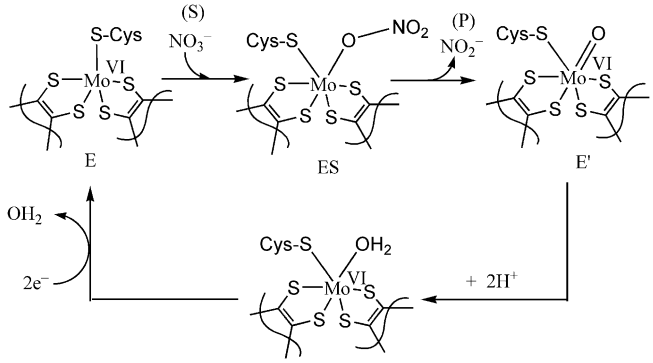

Scheme 1. Simplified nitrate reductase catalytic cycle.[8a]

We have recently reported[10] a functional nitrate reduction (Scheme 2) using 1,2-dicyanoethylenedithiolate (mnt^{2-}) as a model ligand of molybdopterin. The resulting complex, $[Mo(mnt)_2(SPh)(PPh_3)]^-$ (**1a**), readily responds to the OAT reaction (Scheme 2) with nitrate and follows Michaelis–Menten kinetics,[10] which is a characteristic signature of an enzymatic-type reaction [Equation (2)].

$$E + S \rightleftharpoons [ES]' \rightleftharpoons [ES] \rightarrow [EP]' \rightarrow E' + P \quad (2)$$

[a] Department of Chemistry, Indian Institute of Technology Kanpur,
Kanpur 208016, Uttar Pradesh, India
Fax: +91-512-2597265
E-mail: abya@iitk.ac.in

Supporting information for this article is available on the WWW under http://www.eurjic.org or from the author.

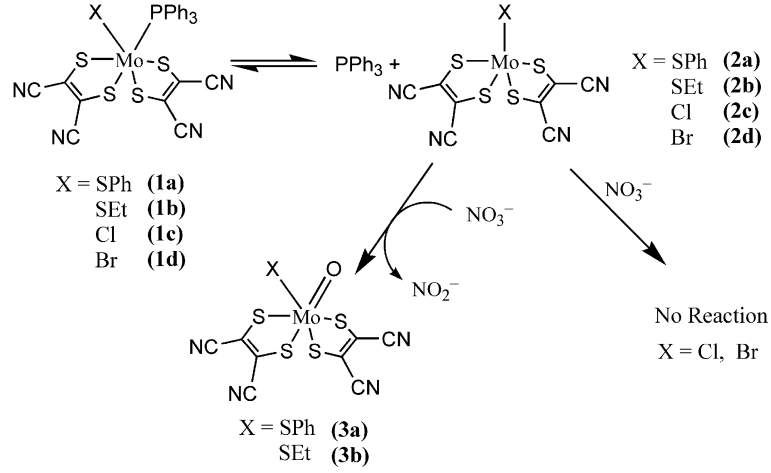

Scheme 2. Reaction scheme of synthetic model complexes.

We proposed[10a] that **1a** is in equilibrium with $[Mo(mnt)_2(SPh)]^-$ (**2a**) in solution and that the reaction starts upon dissociation (as shown by ^{31}P NMR spectroscopy) of PPh_3 from **1a** to form the active pentacoordinate species **2a**, which is responsible for nitrate reduction. Interestingly, we also observed that when the thiolate group is replaced by halide, both the chlorido analog $[Mo(mnt)_2(Cl)(PPh_3)]^-$ (**1c**) and the bromido derivative $[Mo(mnt)_2(Br)(PPh_3)]^-$ (**1d**) are inactive in the nitrate reduction reaction. Hofmann has recently reported[11] a detailed DFT study on several model complexes of Mo-dependent nitrate reductases. He addressed the reactivity difference in **1a** and **1c** with nitrate towards the OAT reaction.[10a] Nevertheless, these calculations failed to provide a plausible explanation for the reactivity difference that occurs upon simply changing the axial ligation at the Mo center from thiolato to chloride (Scheme 2).

To understand this different reactivity of very similar Mo complexes toward nitrate, we decided to extend our experimental work.[10b] Thus, we found that $[Mo(mnt)_2(SEt)(PPh_3)]^-$ (**1b**) behaves similarly to **1a** by also generating $[Mo(mnt)_2(SEt)]^-$ (**2b**) upon dissociation of PPh_3, thereby creating the all-important vacant site for nitrate to bind, although it reacts faster than **1a**. Complex **2b** therefore contains an aliphatic thiol close to the cysteinyl thiolate coordination site of the native protein. The presence of nitrate or another such ionic ligand allows complete dissociation of the bound PPh_3 from the molybdenum center in complexes **1**, whereas in the absence of any such external ion or ligand, the bound PPh_3 is only partially dissociated, and the complexes containing bound and unbound PPh_3 remain in equilibrium. We have reported[10b] previously that the addition of nitrate promotes the release of bound PPh_3 to produce free pentacoordinate species of the type $[Mo^{IV}(X)(mnt)_2]^-$ [X = Cl (**2c**), Br (**2d**)], although these complexes do not go on to promote nitrate reduction even upon binding of nitrate at the available vacant site. To understand the cause of this difference in activity we extended our studies; the results obtained are presented herein. All the complexes containing bound and unbound PPh_3 considered in the present theoretical calculations, along with their respective compound numbers, are tabulated in Table 1.

Table 1. Lists of structures and compound numbers.

Complex	Compound number
$[Mo^{IV}(mnt)_2(SPh)(PPh_3)]^-$	**1a**
$[Mo^{IV}(mnt)_2(SEt)(PPh_3)]^-$	**1b**
$[Mo^{IV}(mnt)_2(Cl)(PPh_3)]^-$	**1c**
$[Mo^{IV}(mnt)_2(Br)(PPh_3)]^-$	**1d**
$[Mo^{IV}(mnt)_2(SPh)]^-$	**2a**
$[Mo^{IV}(mnt)_2(SEt)]^-$	**2b**
$[Mo^{IV}(mnt)_2(Cl)]^-$	**2c**
$[Mo^{IV}(mnt)_2(Br)]^-$	**2d**
$[Mo^{VI}O(mnt)_2(SPh)]^-$	**3a**
$[Mo^{VI}O(mnt)_2(SEt)]^-$	**3b**

It is thought that the nature of the axial ligand may tune the reactivity of the model complexes and thereby affect their OAT reaction. To understand the mechanistic aspects of this reaction with specific axial ligation, we extended our work to include density functional theory (DFT) calculations. Several previous reports have dealt with model systems for the active sites of molybdoenzymes, especially DMSO reductase and TMNO reductase.[12] Furthermore, we have recently shown the nature of the Michaelis complex and the mechanistic pathway for the oxidation of sulfite to sulfate by sulfite oxidase[13] using DFT methods. A DFT investigation has been reported[12c] for nitrate reductase by using $[Mo(SMe)(S_2C_2Me_2)]^-$ as a model complex and with a protein environment model, although the nature of the first transition state – [ES]′ in Equation (2) – prior to the ES formation was not discussed. We have computed the nature of the Michaelis complexes and the gas-phase potential energy surface for the nitrate reduction by synthetic model complexes (**1a** and **1b**) and evaluated the effect of the medium's dielectric constant on the reaction pathway.

Results and Discussion

Electronic Structure Calculation on the PPh_3 Dissociation Step

Based on evidence obtained from the experimental work, we considered that complexes **1a**–**d** undergo PPh_3 dissociation and are in equilibrium with **2a**–**d**, respectively, in solution. As they contain the free binding site, which is necessary for the OAT reaction to occur, pentacoordinate complexes **2a**–**d** should be capable of binding nitrate and reducing it. However, we found that only **1a** and **1b** react with nitrate following Michaelis–Menten kinetics, which indicates that the reaction proceeds via a stable intermediate like ES [see Equation (2)]. Complexes **1c** and **1d**, in contrast, do not react with nitrate. To understand this reactivity difference, we performed electronic structure calculations on **1a**–**d** and **2a**–**d**. The initial geometries of **1a**–**d** were obtained from their crystal structures and the geometries of **2a**–**d** were assumed to involve a square-pyramidal coordination environment of the Mo center with axial ligation of X (X = SPh, SEt, Cl and Br). The two mnt ligands are located in the basal plane and maintain the geometrical parameters of mnt found in **1a**–**d**. The geometries were optimized to local minima by several optimization procedures in the gas phase, and the lowest energy minima were then considered for further calculations. The optimized gas-phase geometries of **1a**–**d** and **2a**–**d** are shown in Figures 1 and 2, respectively. The changes in energy (ΔG and ΔH) for the PPh_3 dissociation steps of **1a**–**d** are listed in Table 2.

The DFT (B3LYP) optimized gas-phase geometries of **1a** and **1b** were found to be in agreement with the geometries obtained from the respective crystal structures (see Figure 1). Both **1a** and **1b** adopt a trigonal-prismatic geometry with Mo–S(dithiolene) bond lengths in the range of 2.402–2.418 Å and Mo–P bond lengths of 2.664 and 2.669 Å for **1a** and **1b**, respectively. The Mo–SPh bond (2.455 Å) is slightly longer than the Mo–SEt bond (2.416 Å), and the P–Mo–SR angle is around 75° in both cases. The optimized gas-phase geometries of **1c** and **1d** (Figure 1) also match well with the geometries obtained from the crystal structures and are very similar to that of **1a**. The only difference lies in the Mo–P distance (2.619 Å), which is slightly shorter than that in **1a**. The optimized Mo–Cl and Mo–Br bond lengths are 2.519 and 2.667 Å, respectively, which are longer than normal.[14]

The optimized gas-phase geometries of **2a**–**d** show a highly symmetrical square-pyramidal coordination environment around the Mo center, with axial Mo–SPh and Mo–SEt bond lengths of 3.322 and 2.304 Å, respectively. The optimized geometries of **2c** and **2d** are very similar to that of **2a**, the only difference being the axial Mo–X [X = Cl (2.283 Å) and Br (2.421 Å)] bond lengths. All the active states for **2a**–**d**, as generated by phosphane dissociation, are very similar as regards the $\{Mo(mnt)_2\}$ unit but vary in their axial ligation. The dihedral angle of the four dithiolene sulfur atoms is zero, thus indicating the symmetric disposition of the two mnt ligands, with Mo around 0.77 Å

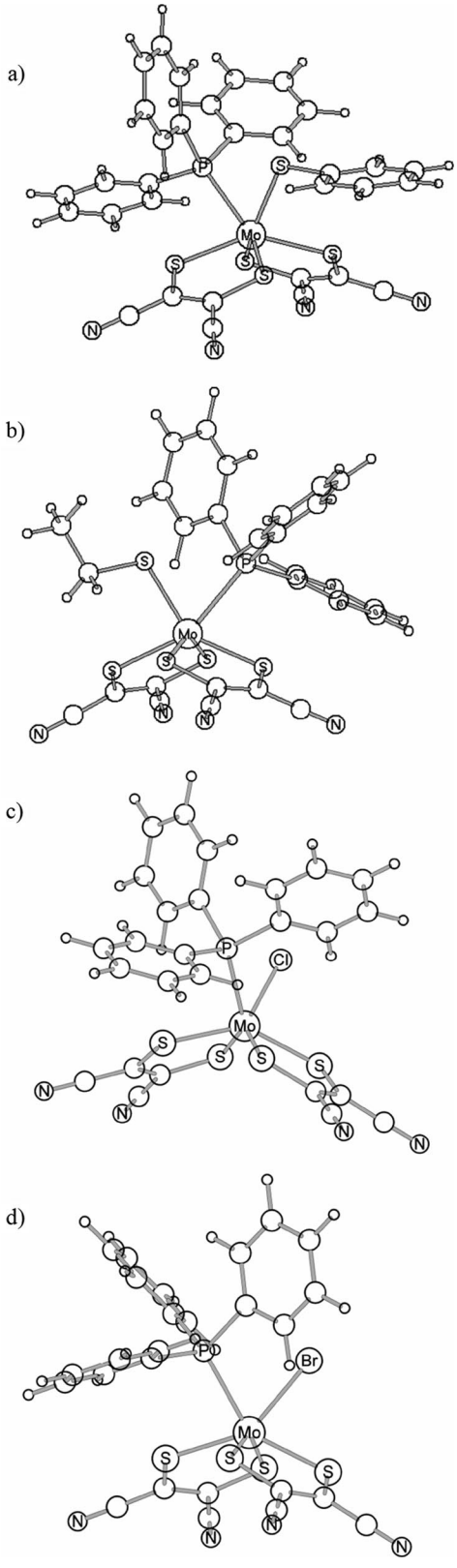

Figure 1. Optimized gas-phase structures of: (a) $[Mo(mnt)_2SPh(PPh_3)]^-$ (**1a**; average Mo–$S_{dithiolene}$: 2.410 Å; Mo–S_{SPh}: 2.455 Å; Mo–P: 2.664 Å); (b) $[Mo(mnt)_2SEt(PPh_3)]^-$ (**1b**; average Mo–$S_{dithiolene}$: 2.415 Å; Mo–S_{Set}: 2.416 Å; Mo–P: 2.669 Å; (c) $[Mo(mnt)_2Cl(PPh_3)]^-$ (**1c**; average Mo–$S_{dithiolene}$: 2.392 Å; Mo–Cl: 2.519 Å; Mo–P: 2.619 Å); (d) $[Mo(mnt)_2Br(PPh_3)]^-$ (**1d**; average Mo–$S_{dithiolene}$: 2.401 Å; Mo–Br: 2.667 Å; Mo–P: 2.619 Å).

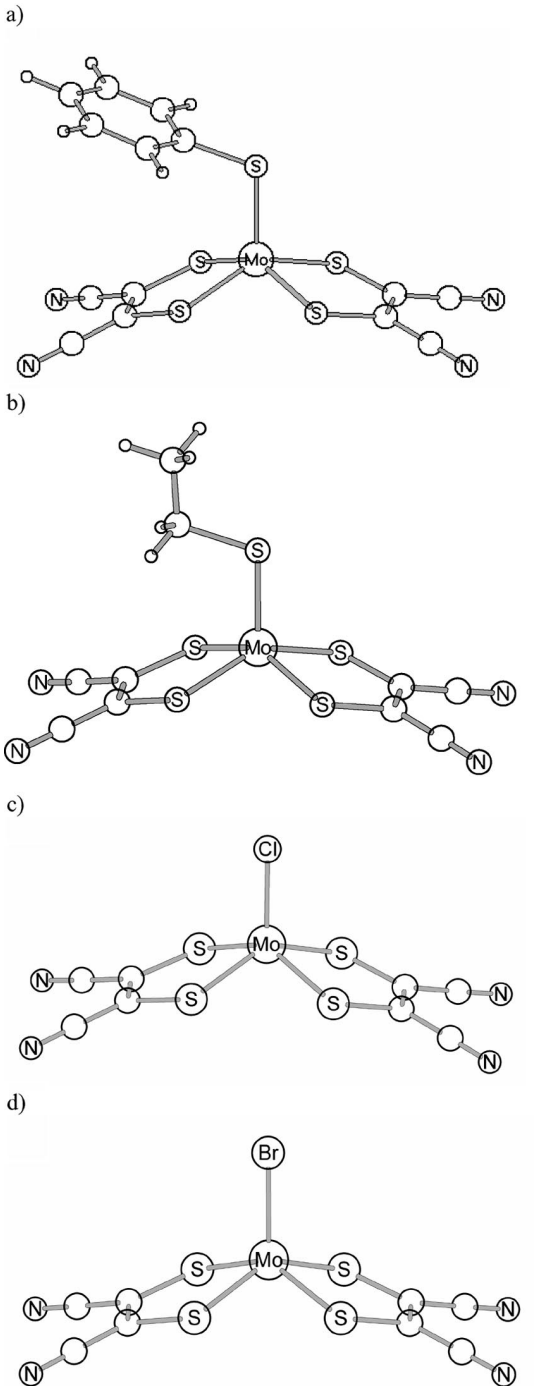

Figure 2. Optimized gas-phase molecular structures of: (a) $[Mo(mnt)_2SPh]^-$ (**2a**; average Mo–$S_{dithiolene}$: 2.365 Å; Mo–S_{SPh}: 2.322 Å); (b) $[Mo(mnt)_2SEt]^-$ (**2b**; average Mo–$S_{dithiolene}$: 2.367 Å; Mo–S_{SEt} 2.304 Å); (c) $[Mo(mnt)_2Cl]^-$, (**2c**; average Mo–$S_{dithiolene}$: 2.361 Å; Mo–Cl 2.283 Å); (d) $[Mo(mnt)_2Br]^-$ (**2d**; average Mo–$S_{dithiolene}$: 2.363 Å; Mo–Br 2.421 Å). C and H atoms are not labeled for clarity.

above the plane of these atoms. The Mo–S(dithiolene) bond lengths vary in the range 2.362–2.371 Å. The phenyl group is oriented parallel and the ethyl group bisects one dithiolene ligand. This is due to weak hydrogen-bonding interactions between ethyl or phenyl hydrogen atoms and the dithiolene sulfur atoms. The geometries of **2a**–**d** are in good agreement with that of the previously reported enzyme model.[11,12c]

Table 2. Energy change during the PPh_3 dissociation steps of **1a**–**d**.

Complex	ΔH [kcal mol^{-1}]	ΔG [kcal mol^{-1}]
1a + NO_3^-	0.00	0.00
2a + NO_3^- + PPh_3	–0.06	–16.3
1b + NO_3^-	0.00	0.00
2b + NO_3^- + PPh_3	–0.06	–15.8
1c + NO_3^-	0.00	0.00
2c + NO_3^- + PPh_3	0.09	–14.8
1d + NO_3^-	0.00	0.00
2d + NO_3^- + PPh_3	–0.13	–15.1

The most interesting result obtained for complexes **1a**–**d** after dissociation of PPh_3 concerns the enthalpy change (ΔH, Table 2), which is very small (nearly zero) in all cases, and the free energy changes, which are much more negative. This indicates that the PPh_3 dissociation step is an equilibrium process and that this dissociation is energetically favorable due to this entropy change. Thus, the PPh_3 dissociation process is energetically equally accessible for all complexes **1a**–**d**. The structural similarity of **1a**–**d**, as obtained from the crystal structures and the optimized gas-phase geometries, strongly suggests that they are likely to have similar structures in solution and that the long Mo–P bond can easily be dissociated, which is in agreement with the experimental findings.[10] If the optimized gas-phase geometries of **2a**–**d** retain a similar geometry in solution to **2a** and **2b** after PPh_3 dissociation, they can be considered as the best analogue of the active site of nitrate reductase (Figure 2).

The structural and energetic similarities of **2a**–**d** found by gas-phase geometry optimization suggest that their electronic environment is not affected by the spatial arrangement of the dithiolene ligand, therefore the active states of **1c** and **1d** formed after PPh_3 dissociation should undergo an OAT reaction with nitrate with the same ease as those species formed by PPh_3 dissociation from **1a** and **1b**. The experimental ^{31}P NMR spectroscopic results indeed show that **1a**–**d** undergo PPh_3 dissociation with equal ease, therefore the reactivity difference must be due to differences in their electronic structures governed by changes in axial ligation. To understand this aspect of the reactivity difference, additional single-point population analysis calculations were carried out in the gas phase by using the same method and a higher level basis set (6-311G*+ for the C, H, N, O, P, Cl and Br atoms and LANL2DZ for the Mo atom). A calculation with the 6-31G*+/LANL2DZ basis set also generates very similar results (see Figure S1 in the Supporting Information). It is known that for the OAT reaction in the family of DMSO reductases, the active species responsible for ES formation is a pentacoordinate Mo^{IV} species, and the potential electron-donor orbital is the $d_{xy}(Mo^{IV})$ orbital. This suggests a one-step two-electron coupled OAT reaction leading to full oxidation of Mo^{IV} to Mo^{VI}. The assignment of this electron-donating MO was made on the

basis of its composition and by visual inspection of its localized orbital. The coordinate frames for all the compounds were assigned by visual inspection of the d_{z^2} and d_{xy} orbitals. Selected frontier molecular orbitals estimated from a Mulliken population analysis calculation in the gas phase are shown in Figure 3.

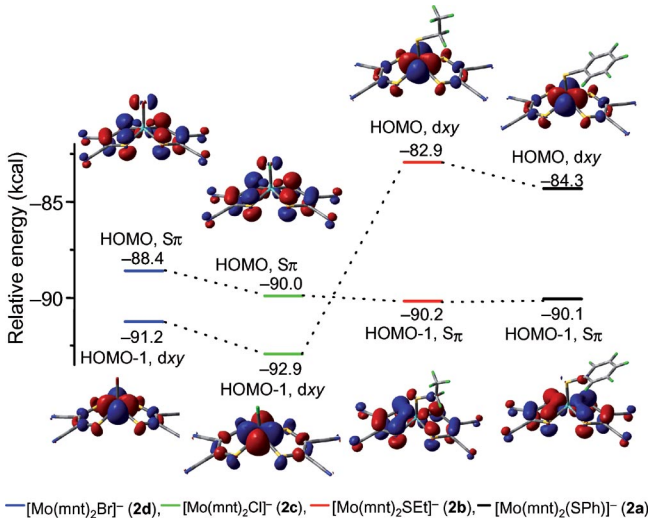

Figure 3. Relative molecular orbital energy level diagram and FMO plot (only the HOMO and HOMO-1 are shown). Basis sets: 6-311G*+ for the C, H, N, O, P, Cl and Br atoms and LANL2DZ for the Mo atom.

The molecular orbital analysis produced interesting results. Thus, the HOMOs of **1a** and **1b** are predominantly the d_{xy}(Mo) orbital, which is the potential electron donor, and the HOMO-1 of **1a** and **1b** originate from an antibonding interaction between the π(S) and π(C=C) orbitals of the dithiolene ligand. The HOMO-1 orbitals of **1a** or **1b** have nearly the same energy, and the HOMOs of **1a** and **1b** are destabilized by 5.8 and 7.3 kcal, respectively, with respect to their HOMO-1 orbitals. These results indicate that when an oxo group of nitrate binds to the Mo center, electron transfer from the HOMO (d_{xy}) to the nitrate coupled with atom transfer (oxygen) from nitrate to Mo can take place. The destabilization of the HOMO of **1b** by 1.4 kcal with respect to that of **1a** supports the experimental findings that **1b** undergoes a faster OAT reaction than **1a**. The situation with the corresponding chlorido (**1c**) and bromido (**1d**) derivatives is rather different, however. Thus, there is an alteration of the population between the two consecutive HOMOs with respect to **1a**: the HOMOs of **1c** and **1d** are π(dithiolene) orbitals and are stabilized by 5.7 and 4.1 kcal, respectively, with respect to the HOMO of **1a**. The HOMO-1 orbitals of **1c** and **1d** are predominantly d_{xy}(Mo) orbitals and are stabilized by 2.8 and 2.5 kcal, respectively, with respect to their respective HOMOs. The potential donor redox orbital is the $d_{xy}(Mo^{IV})$ orbital, which is responsible for the two-electron enzymatic redox reaction. The accessibility of this orbital is the most important issue, however, and the changes in the energy order of the HOMO and HOMO-1 for **2c**,**d** clearly indicate their lack of accessibility. These changes in the positions of these orbitals are retained even when using a solvent dielectric with additional single-point calculations. This type of population alteration is caused by the atomic orbital energy only because all the active states are structurally similar. Using DFT calculations, Holm and Kirk recently observed[15] similar changes in the energy order of the HOMO(ligand) and HOMO-1(d_{xy}, Mo) for $[Mo(OMe)(dithiolene)_2]^-$, a square-pyramidal model complex of DMSO reductase. The twisting of the dithiolene ligand was found to be a property of the protein environment, which induces an interaction between the ligand and d_{xy}(Mo) orbital that destabilizes the latter, thereby facilitating oxidation of the reduced active site and providing substrate access to the redox orbital.

There is no protein environment in our synthetic model system. The experimental results were evaluated in a non-coordinating less polar solvent (dichloromethane), so it is likely that the active states of all the model complexes **2a**–**d** exhibit a similar structure in solution to that we have established by gas-phase optimization. The thiolate ligation in the axial position of square-pyramidal complexes **2a**,**b** satisfies the electronic requirement whereby the redox orbital [d_{xy}(Mo)] in the HOMO must be easily accessible for **2a**,**b** to undergo a facile enzymatic OAT reaction with nitrate. When the apical ligation is changed from thiolate to halide (Cl or Br), however, the orientation of the electronic population is changed in such a way that the redox orbital [d_{xy}(Mo)] is now the HOMO-1 and so is not accessible. This may be the main reason why **2c**,**d** do not undergo an OAT reaction with nitrate despite possessing a structure similar to **2a**,**b**. Thus, the nature of the axial ligation tunes the electronic criteria and also the reactivity.

Searching for the Michaelis Complex

During our search for the Michaelis complex in the reaction of **1a**–**d** with nitrate, we carried out several optimization processes to identify the stationary point of the nitrate-bound ES complex with respect to the native enzyme. We found that **2a** and **2b** form a stable intermediate (**ESa** and **ESb**, respectively; Figure 4). Complexes **ESa** (ΔG = 11.4 and ΔH = 14.4 kcal mol^{-1}) and **ESb** (ΔG = 17.6 and ΔH = 19.0 kcal mol^{-1}) are relatively stable intermediates where nitrate is weakly bonded to the Mo center with an Mo–ONO_2 distance of 2.122 Å for **ESa** and 2.149 Å for **ESb** and an O–NO_2 distance of 1.334 and 1.327 Å, respectively, which represent an elongation of around 0.05 Å. Because of the direct coordination of nitrate to the Mo center through its oxo group, the coordination number around the Mo center increases to impose a distorted octahedral geometry to **ESa** and **ESb** with all the Mo–S(dithiolene) distances falling in the range 2.414–2.477 Å, an Mo–SPh bond length of 2.444 Å in **ESa** and an Mo–SEt bond length of 2.401 Å in **ESb**. The S(Ph/Et)–Mo–ONO_2 angles are around 79°. The greater stability of **ESb** with respect to **ESa** is imposed by the additional $O_2NO\cdots HCH(Me)S$ hydrogen-bonding interaction of 2.222 Å. Thus, **ESa** and **ESb** could

be considered to be the best representative synthetic models of the substrate-bound enzyme–substrate complex, or Michaelis complex, before the OAT reaction for nitrate reductase. The geometries of **ESa** and **ESb** are in good agreement with that of the previously reported[11,12c] enzyme–substrate complex $[Mo(S_2C_2Me_2)_2SCH_3]^-$ for the reduction of nitrate obtained computationally.

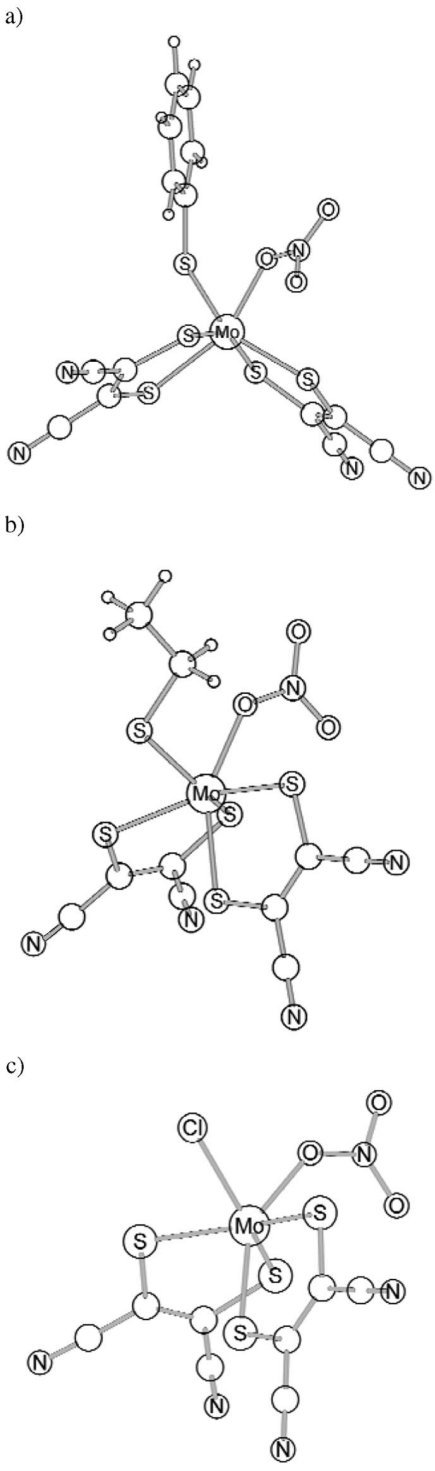

Figure 4. Gas-phase-optimized molecular structures of: (a) **ESa** [average $Mo–S_{dithiolene}$: 2.434 Å; $Mo–S_{SPh}$: 2.445 Å; $Mo–O(NO_2)$: 2.122 Å]; (b) **ESb** [average $Mo–S_{dithiolene}$: 2.441 Å; $Mo–S_{Set}$: 2.401 Å; $Mo–O(NO_2)$: 2.414 Å]; (c) **Esc** [average $Mo–S_{dithiolene}$: 2.449 Å; Mo–Cl: 2.542 Å; $Mo–O(NO_2)$: 2.091 Å]. C and H atoms are not labeled for clarity.

After several optimization attempts, a gas-phase stationary point was found for nitrate-bound **2c**, albeit at high energy (**Esc**; ΔG = 225.4 and ΔH = 229.8 kcal mol^{-1}; Figure 4). **ESc** adopts a distorted octahedral geometry with an average Mo–S(dithiolene) bond length similar to that in **ESa** and an $Mo–ONO_2$ distance of 2.091 Å, which is slightly shorter than that in **ESa**, thus indicating that the substrate is strongly bound to the Mo center. Despite several optimization attempts, however, we failed to obtain the optimized geometry of nitrate-bound **2d**, which indicates that a stationary point, even one with high energy, does not exist for the ES of **2d**.

Any enzymatic reaction requires a stable enzyme–substrate complex to be formed as the first step. Although **2c** forms such a complex (**ESc**) that is structurally similar to **ESa**,**b**, it is energetically very unstable. This result indicates that, because of this high destabilization, if **ESc** is formed upon attack of the substrate it will rapidly decompose before onset of the OAT reaction. This type of ES complex may be a good example of a non-productive ES because the redox orbital needed for a reaction to occur is also inaccessible. The population analysis and the energetics of the reaction of **1c**,**d** with nitrate are in good agreement with the previous experimental results,[10] where **2c**,**d** are immediately converted into the tris(complex) upon addition of nitrate to a dichloromethane solution due to the highly unstable nature of ES and the poor accessibility of the redox orbital.

Reaction Pathway for the Reaction of $[Mo^{IV}(mnt)_2(SPh)(PPh_3)]^-$ and $[Mo^{IV}(mnt)_2(SEt)(PPh_3)]^-$ with Nitrate

The population analysis of the molecular orbital and the nature of the ES complexes have clearly established that **1a**,**b** form stable ES complexes towards the OAT reaction but that **1c**,**d** cannot undergo such an OAT reaction with nitrate. This is in good agreement with our previously reported experimental results. At this stage, we extended our calculations with systems **1a**,**b** in order to determine the complete mechanistic pathway and all the intermediate transition states and intermediates in the OAT reaction with nitrate. The complete reaction pathway for nitrate reduction by the synthetic model complexes **1a** and **1b** was carried out with respect to nitrate reductase. The relative energy profile for the reaction of **1a** with nitrate was computed with the fully optimized reaction coordinates in the gas phase (see Figure 5). The optimized geometries are shown in Figure 6. The reaction of **1a** with nitrate involves an initial dissociation of **1a** to form **2a** and PPh_3. This step generates the active state, which passes through the transition state **TS1a**, a substrate-bound intermediate (**ESa**), a second transition state (**TS2a**), and finally produces **3a** and nitrate. The reaction of **1b** with nitrate occurs in a similar manner. The relative energy profile for the reaction of **1b** with nitrate

was computed with the fully optimized reaction coordinates in the gas phase (see Figure 7). The optimized geometries are shown in Figure 8. The optimized values of selected bond lengths in these states are listed in Table 3.

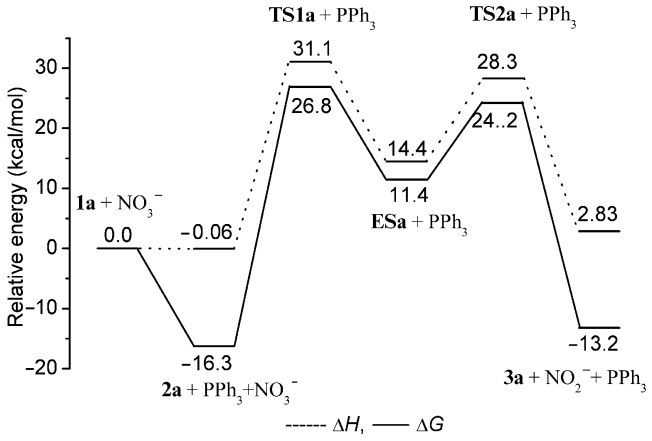

Figure 5. Gas-phase-calculated reaction pathways for the reaction of $[Mo(mnt)_2SPh(PPh_3)]^-$ with NO_3^- at 298 °K.

The first step for model complex **1a** is the reversible dissociation of PPh_3 to generate the active state. For the reaction of **1a** (ΔG = 0.0 and ΔH = 0.0 kcal mol^{-1}) with nitrate, complex **2a** (ΔG = –15.8 and ΔH = –0.06 kcal mol^{-1}) is the active state for the atom-transfer reaction relevant to nitrate reductase. The first step of the OAT reaction is then followed by the binding of nitrate to the molybdenum center of **2a** to form a stable intermediate **ESa** (ΔG = 11.4 and ΔH = 14.4 kcal mol^{-1}) through a potential energy barrier for the first transition state **TS1a** (ΔG = 26.8 and ΔH = 31.1 kcal mol^{-1}; Figure 6). **TS1a** is 12 kcal mol^{-1} higher in energy (ΔG = 72.2 kcal mol^{-1}) than the active state **2a**. The geometry of **TS1a** does not affect the active state **2a**, where nitrate is weakly bound (Mo–ONO_2: 3.093 Å; O–NO_2: 1.281 Å) to the Mo center, and all the Mo–S bond lengths are essentially the same as in the reactant, very much – only the axial SPh group is moved by 12° from the perpendicular position of the basal plane of the square-pyramidal geometry of **2a**. The formation of **TS1a** is facilitated by the special orientation of nitrate due to the $O_2NO\cdots HC_6H_4S$ hydrogen-bonding interaction (2.147 Å). No information regarding the geometry of the first transition complex before ES formation[12c] could be established for this model complex.

The second step of the OAT reaction of **2a** passes through the transition state **TS2a** (ΔG = 24.2 and ΔH = 28.3 kcal mol^{-1}; Figure 6), which has Mo–ONO_2 and O–NO_2 bond lengths of 1.816 and 1.871 Å, respectively. **TS2a** adopts a distorted octahedral geometry with an Mo–SPh bond length of 2.664 Å and has only one imaginary frequency of –175 cm^{-1}, which confirms the first-order saddle-point character between the two minima. This imaginary frequency corresponds to the stretching vibration mode of the Mo–ONO_2 and O–NO_2 bonds. **TS2a** forms the product (**3a**; ΔG = –13.2 and ΔH = 2.83 kcal mol^{-1}; Figure 6) through an energy barrier of 13.9 kcal mol^{-1} (ΔG = 12.8 kcal mol^{-1}), which consists of the breaking of the O–NO_2 bond and the formation of the Mo–ONO_2 bond.

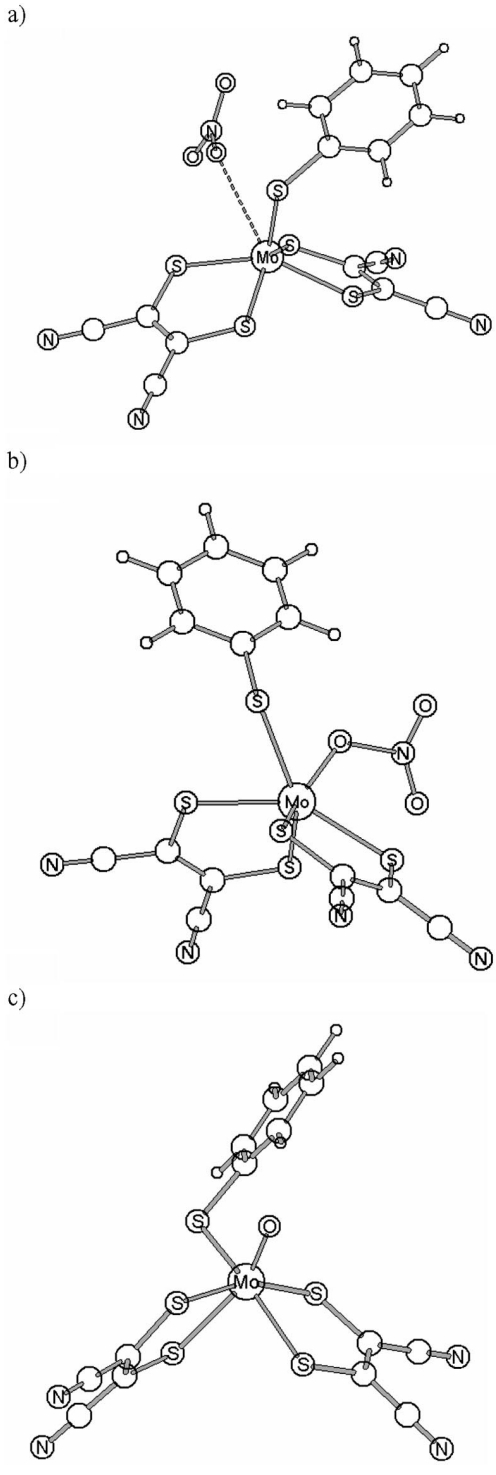

Figure 6. Gas-phase-optimized molecular structures of: (a) **Ts1a** [average Mo–$S_{dithiolene}$: 2.378 Å; Mo–S_{SPh}: 2.368 Å; Mo–$O(NO_2)$ 3.090 Å]; (b) **Ts2a** [average Mo–$S_{dithiolene}$: 2.463 Å; Mo–S_{SPh}: 2.664 Å; Mo–$O(NO_2)$: 1.816 Å]; (c) $[Mo^{VI}O(mnt)_2SPh]^-$ [**3a**; average Mo–$S_{dithiolene}$: 2.451 Å; Mo–$S_{dithiolene}$ (*trans* to oxo): 2.632 Å; Mo–S_{SPh}: 2.470 Å; Mo–O_t: 1.712 Å]. C and H atoms are not labeled for clarity; subscript t: terminal.

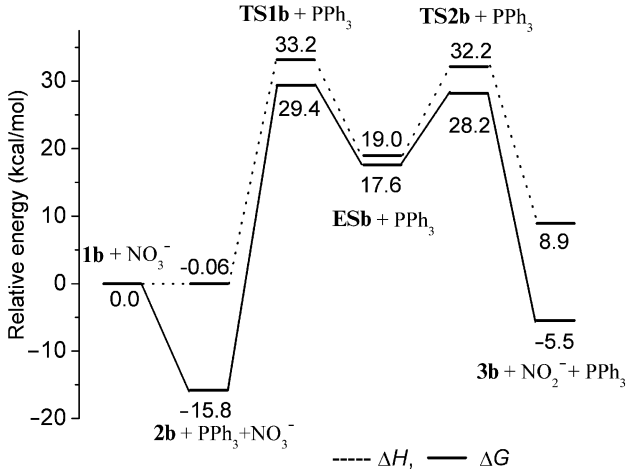

Figure 7. Gas-phase-calculated reaction pathways for the reaction of $[Mo(mnt)_2SEt(PPh_3)]^-$ (**1b**) with NO_3^-.

Complex **3a** has a distorted octahedral geometry with a terminal double-bonded oxo group (Mo–O_t: 1.712 Å) *cis* to the thiolato ligand at the molybdenum center, thus indicating that the atom-transfer reaction is complete.

The OAT reaction of **1b** with nitrate is very similar in nature to that between **1a** and nitrate (Figure 7). The geometry-optimized molecular structures are shown in Figure 8.

The first step is, once again, the reversible dissociation of $PPh_3$to produce the active state **2b** (ΔG = –15.8 and ΔH = –0.06 kcal mol^{-1}), the geometrical features of which have been discussed above. The enzymatic OAT reaction starts upon initial attack of the nitrate at the Mo center of **2b**, passing through an energy barrier of ΔH = –28.8 (ΔG = 49.0 kcal mol^{-1}), to form the first transition state **TS1b** (ΔG = 29.4 and ΔH = 33.2 kcal mol^{-1}; Figure 8). Nitrate is weakly bound in **TS1b**, with an Mo–ONO_2 bond length of 3.148 Å, Mo–S(dithiolene) bond lengths ranging from 2.353 to 2.396 Å, and an apical Mo–SEt bond length of 2.368 Å. The structural parameters of **TS1b** are very similar to those of **TS1a**, with a similar type of hydrogen-bonding interaction between nitrate and the hydrogen atom of the SEt group. After crossing the transition state **TS1b**, the reaction path leads to the stable intermediate **ESb** (ΔG = 17.6 and ΔH = 19.0 kcal mol^{-1}), the nature of which has also been discussed in the previous section (Figure 4).

The next step of the OAT reaction of **2b** gives the product (**3b**; ΔG = –5.5 and ΔH = 8.9 kcal mol^{-1}) through a second energy barrier of ΔH = 14.2 (ΔG = 10.6 kcal mol^{-1}) for the second transition state **TS2b** (ΔG = 28.2 and ΔH = 32.2 kcal mol^{-1}; Figure 8). **TS2b** has a distorted octahedral geometry with an Mo–SEt bond length of 2.505 Å and all the Mo–S(dithiolene) bond lengths in the range 2.446–2.528 Å. **TS2b** has only one imaginary frequency of –228 cm^{-1}, which confirms the first-order saddle-point character between the two minima. This imaginary frequency corresponds to the stretching vibration mode of the Mo–ONO_2 and O–NO_2 bonds. **TS2b** goes on to form the product by a breaking of the O–NO_2 bond and formation

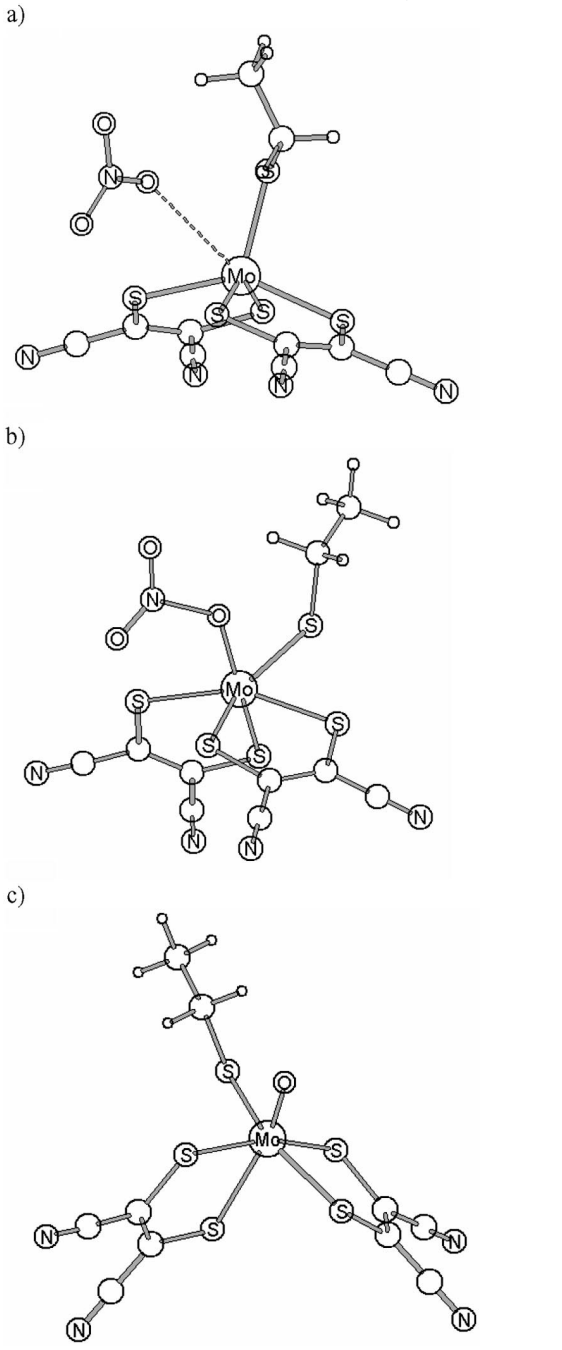

Figure 8. Gas-phase-optimized molecular structures of: (a) **Ts1b** [average Mo–$S_{dithiolene}$: 2.399 Å; Mo–S_{Set}: 2.328 Å; Mo–$O(NO_2)$: 3.148 Å]; (b) **Ts2b** [average Mo–$S_{dithiolene}$: 2.481 Å; Mo–S_{Set}: 2.505 Å; Mo–$O(NO_2)$: 1.838 Å]; (c) $[Mo^{VI}O(mnt)_2]^-$ [**3b**; average Mo–$S_{dithiolene}$: 2.465 Å; Mo–$S_{dithiolene}$ (*trans* to oxo): 2.648 Å; Mo–S_{Set}: 2.439 Å; Mo–O_t 1.716 Å]. C and H atoms are not labeled for clarity; subscript t: terminal.

of the Mo–O_t bond. The geometry of complex **3b** is very similar to that of **3a**, with a terminal Mo–O_t bond length of 1.716 Å.

The enthalpy changes resulting from the overall reaction of **1a** and **1b** with nitrate are slightly positive (2.83 and 8.9 kcal mol^{-1}, respectively) and the free-energy changes more negative (–13.2 and –5.5 kcal mol^{-1}, respectively),

Table 3. Selected bond lengths in the optimized geometries.

	Distances [Å]							
	Mo–S1	Mo–S2	Mo–S3	Mo–S4	Mo–S5 (SR)	Mo–ONO_2	O–NO_2	Mo–O_t
Reaction of $[Mo(mnt)_2(SPh)(PPh_3)]^-$ with nitrate								
1a	2.407	2.417	2.414	2.403	2.455	–	–	–
2a	2.362	2.362	2.368	2.368	2.322	–	–	–
TS1a	2.392	2.362	2.378	2.381	2.368	3.090	1.281	–
ESa	2.423	2.414	2.477	2.423	2.444	2.122	1.334	–
TS2a	2.450	2.465	2.470	2.468	2.664	1.861	1.871	–
3a	2.477	2.456	2.632[a]	2.422	2.470	–	–	1.712
Reaction of $[Mo(mnt)_2(SEt)(PPh_3)]^-$ with nitrate								
1b	2.412	2.422	2.418	2.408	2.416	–	–	–
2b	2.363	2.363	2.371	2.371	2.304	–	–	–
TS1b	2.387	2.406	2.353	2.396	2.328	3.148	1.278	–
ESb	2.428	2.438	2.430	2.467	2.401	2.149	1.327	–
TS2b	2.528	2.446	2.468	2.485	2.505	1.838	1.830	–
3b	2.423	2.483	2.648[a]	2.491	2.439	–	–	1.716

[a] *trans* to terminal oxo group.

which suggests that each step of this atom-transfer reaction is highly dependent on the entropy factor. The stable intermediates **ESa** and **ESb** are in equilibrium with the active states (**2a** and **2b**, respectively) in a high-energy process that is driven by the entropy factor and the concentration of the substrate. The product-formation step from **ESa** to **3a** is energetically a highly favorable process (ΔG = –24.6 and ΔH = –12.1 kcal mol^{-1}). Similarly, the product-formation step from **ESb** to **3b** is also energetically highly favorable (ΔG = –23.1 and ΔH = –10.1 kcal mol^{-1}). This product-formation step is unidirectional and influences the forward reaction rate constant of the previous equilibrium (**ESa** and **ESb** formation steps) in such a manner that this rate constant increases. Once **ESa** and **ESb** have formed, they immediately go on to form the respective products by the atom-transfer reaction step due to the endothermic nature of this step. The stability of **ES** also influences the rate of the overall reaction – **1b** reacts faster as the lower stability of **ESb** than **ESa** means that it has to overcome a lower potential energy barrier to form the products.

Finally, we evaluated the dielectric effect of the medium on the potential-energy surface by additional single-point calculations using the same method and a higher-level basis set (6-311G*+ for C, H, N, O, P, Cl, and Br and LANL2DZ for Mo). The corrected solvation/energy profiles obtained with the conductor-like screening model[16] (COSMO), with dichloromethane (ε = 8.93) as solvent, for the gas-phase-optimized structures calculated for the reaction of **1a** and **1b** with nitrate are shown in Figure 9. A similar calculation with the 6-31G*+/LANL2DZ basis set generates very similar results (see Supporting Information, Figure S2).

We found that all the intermediates and transition states where an anionic substrate is bonded to an anionic model complex were stabilized by the solvation energy relative to their reactants and products. Both the reactant and product molecules are negatively charged ions in our model system – the reactions involve the association of two negatively charged reactants (**2a** or **2b** and nitrate) – therefore their energies were calculated separately. Although such a reaction proceeds through a localized orbital interaction, the

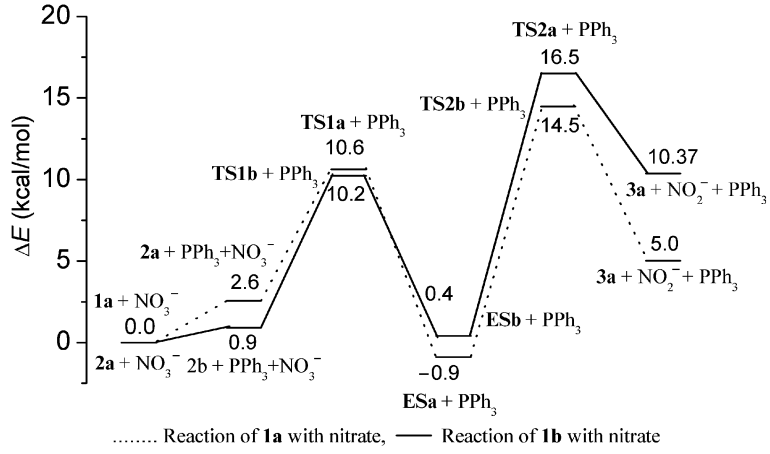

Figure 9. Solvent-corrected energy profile for the reaction of **1a** and **1b** with nitrate at 298 K obtained with the COSMO solvent model by the same method but with the LANL2DZ basis set for Mo and the 6-311G*+ basis set for the remaining atoms. The solvent is dichloromethane.

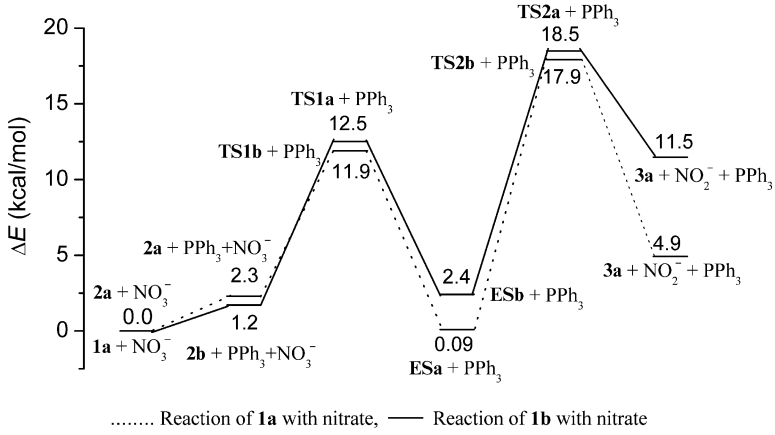

Figure 10. Solvent-corrected energy profile for the reaction of **1a** and **1b** with nitrate at 298 K obtained by the COSMO method with the LANL2DZ basis set for Mo and the 6-311G*+ basis set for the remaining atoms. The solvent dielectric is 5.

association of two negatively charged ions increases the overall energy of the reaction pathway in the gas phase due to the presence of additional intramolecular repulsive interactions in the gas phase. This repulsive interaction between two similarly charged species is stabilized in the continuum model.

The protein environment plays a significant role in the overall reaction pathway by minimizing the potential energy barrier in native proteins. To address this, we evaluated the effect of the dielectric of the medium under study. Medium dielectrics[16] in the range 3–5 are often employed to mimic the protein environment, therefore we chose a value of 5 and performed additional single-point calculations (COSMO) to mimic the effect of the protein environment in the reaction system for our model complexes. The corrected solvation-energy profile obtained with COSMO,[16] by using the LANL2DZ basis set for Mo and the 6-311G*+ basis set for the remaining atoms, for the gas-phase-optimized structures for the reaction of **1a** and **1b** with nitrate are shown in Figure 10. The overall nature of the potential-energy surface and relative energies for all the intermediates, transition states, and products are very similar to those obtained in the reaction medium [dichloromethane (ε = 8.93); Figure 9].

To check the validity of the single-point calculation we carried out additional single-point calculations with the PCM[17] and dipole models[18] using the same method and higher-level basis sets (6-311G*+ for C, H, N, O, P, Cl, and Br and LANL2DZ for Mo). A comparison of the solvent-corrected energy of the reactants, intermediates, transition states, and products with different solvent models is shown in Table 4. A similar calculation with the 6-31G*+/LANL2DZ basis sets generated very similar results (Supporting Information, Table S1).

The PCM model provides a similar stabilization to the continuum model. However, a similar stabilization was not observed in the dipole model because of the inherent consideration of the solute surface in this model. A similar type of solvent-interaction phenomenons has been observed previously for the potential energy surface of sulfite oxidation by a model complex of sulfite oxidase.[13] In the case of the native enzyme, it is expected that the protein environment may play a similar role in minimizing the energy of the catalytic pathway.

Table 4. Relative single-point energies [kcal mol^{-1}] of reactants, intermediates, TSs, and products for the reaction of **1a** and **1b** with nitrate obtained with different solvent models and in the gas phase for gas-phase-optimized geometries with the LANL2DZ basis set for Mo and the 6-311G*+ basis set for the remaining atoms.

	Gas phase	COSMO	PCM	DIPOLE
Reaction of $[Mo(mnt)_2(SPh)(PPh_3)]^-$ with nitrate				
1a + NO_3^-	0	0	0	0
2a + NO_3^- + PPh_3	–0.56	2.56	1.47	2.19
TS1a + PPh_3	30.5	10.7	9.90	33.4
ESa + PPh_3	15.1	–0.89	–1.74	17.3
TS2a + PPh_3	30.1	14.5	0.58	33.6
3a + PPh_3 + NO_2^-	5.32	5.015	4.51	8.48
Reaction of $[Mo(mnt)_2(SEt)(PPh_3)]^-$ with nitrate				
1b + NO_3^-	0	0	0	0
2b + NO_3^- + PPh_3	–0.10	0.91	0.91	1.79
TS1b + PPh_3	33.4	10.2	10.3	36.89
ESb + PPh_3	19.34	0.40	–0.09	23.5
TS2b + PPh_3	34.5	16.5	16.0	37.85
3b + PPh_3 + NO_2^-	13.3	10.3	10.5	16.35

Conclusions

DFT calculations on the synthetic functional model complexes of nitrate reductase are in good agreement with the experimental findings and show that axial thiolate ligation at the Mo center is essential for nitrate reduction activity. A change in axial ligation from thiolate to halide at the molybdenum center causes the participating redox orbital to become energetically less accessible, which means that the reaction with nitrate does not occur. The nature of the ES of all the model complexes has been established, and the reason why halide derivatives do not react with nitrate explained. The higher reaction rate of **2b** with respect to that of **2a** is found to be due to the lower stability of the

ES of **2b**. The complete reaction pathways for the reduction of nitrate with aliphatic and aromatic thiolato-ligated model complexes have been calculated in the gas phase and also with a continuum solvent model. It is expected that the reactivity of the native protein may also be influenced by the nature of the axial ligation. It has been found for the DMSO reductase class of enzymes, for instance, that Nature has chosen different apical (axial) ligation with different donor atoms for different substrates. Thus, DMSO reductase shows reactivity towards both DMSO and TMANO (trimethylamine *N*-oxide), but TMANO reductase does not react with DMSO. The inactivity of any member of this family could be governed by a change in the axial ligation of the Mo cofactor.

Computational Methods

All calculations were performed with the Gaussian 03 package (revision B.04).[19] Molecular orbitals were visualized by using "Gauss View", and geometry-optimized molecular structures were generated by using Diamond 3.1e. All the geometry optimizations were carried out at the density functional theory level. The method used was Becke's three-parameter hybrid exchange functional,[20] with the non-local correlation provided by the Lee, Yang, and Parr expression (B3LYP), and the Vosko, Wilk, and Nuair 1980 correlation functional (III) for local correlations (B3LYP). The 6-311g*+ basis set[21] was used for C, N, S, and H atoms, and the LANL2DZ[22] basis set and LANL2 pseudo potentials of Hay and Wadt[23] for the Mo atom. Transition states were optimized by using the synchronous transit-guided quasi-Newton (STQN) method.[24] The optimized minima and transition-state structures were characterized by harmonic vibration frequency calculations using the same method, where a minimum has no imaginary frequency and a transition state has only one imaginary frequency. The additional single-point calculations were carried out on the gas-phase-optimized geometry for population analysis of the molecular orbital and the dielectric effect of the medium using the same method but higher level basis sets (6-311G*+ for C, H, N, O, P, Cl, and B, and LANL2DZ for Mo). For the medium effect, a solvation correction was carried out with the conductor-like screening model[16] (COSMO) by using dichloromethane as solvent and a temperature of 298 K. Dielectric constants[16] of 3–5 are often employed to mimic the protein environment. We chose a value of 5 for the additional single-point calculations (COSMO) to determine the effect of the protein environment on the synthetic model complexes. The validity of single-point energy calculations with the solvent model was checked with other solvent models such as the PCM[17] and dipole models.[18]

Supporting Information (see footnote on the first page of this article): Molecular orbital counter plot, solvent-corrected energy profile, relative single-point energies with different solvent models and coordinates for the gas-phase-optimized molecular geometry using the DFT method and the 6-31G*+ basis set for C, H, N, O, P, Cl, and Br, and LANL2DZ for Mo.

Acknowledgments

K. P. thanks the Council of Scientific and Industrial Research, New Delhi for providing a doctoral fellowship. S. S. is grateful for research funding with computational facilities from the Department of Science and Technology, New Delhi (SR/S5/BC-01/2006).

[1] *Metal Ions in Biological Systems*, vol. 39 ("Molybdenum and Tungsten: Their Role in Biological Processes") (Eds.: A. Sigel, H. Sigel), Routledge Publisher, New York, USA, **2002**.
[2] K. V. Rajagopalan, *Adv. Enzym.* **1991**, *64*, 215.
[3] A. Thapper, C. Lorber, J. Fryxelius, A. Behrens, E. Nordlander, *J. Inorg. Biochem.* **2000**, *79*, 67.
[4] R. Hille, *Chem. Rev.* **1996**, *96*, 2757.
[5] a) R. Huber, P. Hof, R. O. Duarte, J. J. G. Moura, I. Moura, M.-Y. Liu, J. LeGall, R. Hille, M. Archer, M. J. Romão, *Proc. Natl. Acad. Sci. USA* **1996**, *93*, 8846; b) R. Hille, G. N. George, M. K. Eidsness, S. P. Cramer, *Inorg. Chem.* **1989**, *28*, 4018; c) C. Enroth, B. T. Eger, K. Okamoto, T. Nishino, T. Nishino, E. F. Pai, *Proc. Natl. Acad. Sci. USA* **2000**, *97*, 10723; d) J. J. Truglio, K. Theis, S. Leimkühler, R. Rappa, K. V. Rajagopalan, C. Kisker, *Structure* **2002**, *10*, 115.
[6] a) M. Dixon, E. C. Webb, C. J. R. Throne, K. F. Tipton, *Enzymes*, 3rd ed., Academic Press, New York, **1979**; b) L. G. Howell, I. Fridovich, *J. Biol. Chem.* **1968**, *243*, 5941; c) D. L. Kessler, K. V. Rajagopalan, *J. Biol. Chem.* **1972**, *247*, 6566; d) D. L. Kessler, K. V. Rajagopalan, *Biochim. Biophys. Acta* **1974**, *370*, 399; e) J. L. Johnson, K. V. Rajagopalan, *J. Clin. Invest.* **1978**, *58*, 543; f) S. P. Kramer, J. L. Johnson, A. A. Ribeiro, D. S. Mullington, K. V. Rajagopalan, *J. Biol. Chem.* **1987**, *262*, 16357; g) G. N. George, I. J. Pickering, C. Kisker, *Inorg. Chem.* **1999**, *38*, 2539; h) C. Kisker, H. Schindelin, A. Pacheco, W. A. Wehbi, R. M. Garrett, K. V. Rajagopalan, J. H. Enemark, D. C. Rees, *Cell* **1997**, *91*, 973.
[7] a) H.-K. Li, C. Temple, K. V. Rajagopalan, H. Schindelin, *J. Am. Chem. Soc.* **2000**, *122*, 7673; b) G. N. George, J. Hilton, C. Temple, R. C. Prince, K. V. Rajagopalan, *J. Am. Chem. Soc.* **1999**, *121*, 1256; c) J. M. Dias, M. E. Than, A. Humm, R. Huber, G. P. Bourenkov, H. D. Bartunik, S. Bursakov, J. Calvete, J. Caldeira, C. Carneiro, J. J. G. Moura, I. Moura, M. J. Romao, *Structure* **1999**, *7*, 65; d) J. C. Boyington, V. N. Gladyshev, S. V. Khangulov, T. C. Stadtman, P. D. Sun, *Science* **1997**, *275*, 1305; e) M. Jormakka, S. Tornroth, B. Byrne, S. Iwata, *Science* **2002**, *295*, 1863; f) S. Najmudin, P. J. González, J. Trincão, C. Coelho, A. Mukhopadhyay, N. M. F. S. A. Cerqueira, C. C. Romão, I. Moura, J. J. G. Moura, C. D. Brondino, M. J. Romão, *J. Biol. Inorg. Chem.* **2008**, *13*, 737.
[8] J. M. Dias, M. E. Than, A. Humm, R. Huber, G. P. Bourenkov, H. D. Bartunik, S. Bursakov, J. Calvete, J. Caldeira, C. Carneiro, J. J. G. Moura, I. Moura, M. J. Romao, *Structure* **1999**, *7*, 65–79.
[9] a) B. S. Lim, J. P. Donahue, R. H. Holm, *Inorg. Chem.* **2000**, *39*, 263–273; b) K. B. Musgrave, B. S. Lim, K.-M. Sung, R. H. Holm, B. Hedman, K. O. Hodgson, *Inorg. Chem.* **2000**, *39*, 5238–5247; c) B. S. Lim, R. H. Holm, *J. Am. Chem. Soc.* **2001**, *123*, 1920–1930.
[10] a) A. Majumdar, K. Pal, S. Sarkar, *J. Am. Chem. Soc.* **2006**, *128*, 4196; b) A. Majumdar, K. Pal, S. Sarkar, *Inorg. Chem.* **2008**, *47*, 5360.
[11] M. Hofmann, *J. Biol. Inorg. Chem.* **2007**, *12*, 989.
[12] a) C. E. Webster, M. B. Hall, *J. Am. Chem. Soc.* **2001**, *123*, 5820; b) A. Thapper, R. J. Deeth, E. Nordlander, *Inorg. Chem.* **2002**, *41*, 6695; c) M. Leopoldini, M. Toscano, M. Dulak, T. A. Wesolowski, *Chem. Eur. J.* **2006**, *12*, 2532; d) A. Thapper, R. J. Deeth, E. Nordlander, *Inorg. Chem.* **1999**, *38*, 1015; e) M. A. Pietsch, M. B. Hall, *Inorg. Chem.* **1996**, *35*, 1273; f) M. R. Bray, R. J. Deeth, *Inorg. Chem.* **1996**, *35*, 5720; g) M. R. Bray, R. J. Deeth, *J. Chem. Soc., Dalton Trans.* **1997**, 4005; h) P. Ilich, R. Hille, *J. Chem. Phys.* **1999**, *103*, 5406; i) M. R. Bray, R. J. Deeth, *J. Chem. Soc., Dalton Trans.* **1997**, 1267; j) A. A. Voityuk, K. Albert, S. Kostlmeier, V. A. Nasluzov, K. M. Neyman, P. Hof, M. J. Romao, N. Rosch, *J. Am. Chem. Soc.* **1997**, *119*, 3159; k) A. Voityuk, K. Albert, M. J. Romão, R. Huber, N. J. Rosch, *Inorg. Chem.* **1998**, *37*, 176.
[13] K. Pal, P. K. Chaudhury, S. Sarkar, *Chem. Asian J.* **2007**, *2*, 956.

[14] K. Pal, R. Maiti, P. K. Chaudhury, S. Sarkar, *Inorg. Chim. Acta* **2007**, *360*, 2721.
[15] R. L. McNaughton, B. S. Lim, S. Z. Knottenbelt, R. H. Holm, M. L. Kirk, *J. Am. Chem. Soc.* **2008**, *130*, 4628.
[16] a) P. E. Smith, R. M. Brunne, A. E. Mark, W. F. van Gunsteren, *J. Phys. Chem.* **1993**, *97*, 2009; b) G. Löffler, H. Schreiber, O. Steinhauser, *J. Mol. Biol.* **1997**, *270*, 520; c) F. Ogliaro, S. P. de Visser, S. Cohen, P. K. Sharma, S. Shaik, *J. Am. Chem. Soc.* **2002**, *124*, 2806–2814.
[17] a) M. T. Cancès, B. Mennucci, J. Tomasi, *J. Chem. Phys.* **1997**, *107*, 3032; b) M. Cossi, V. Barone, B. Mennucci, J. Tomasi, *Chem. Phys. Lett.* **1998**, *286*, 253; c) B. Mennucci, J. Tomasi, *J. Chem. Phys.* **1997**, *106*, 5151.
[18] a) L. Onsager, *J. Am. Chem. Soc.* **1936**, *58*, 1486; b) M. W. Wong, M. J. Frisch, K. B. Wiberg, *J. Am. Chem. Soc.* **1991**, *113*, 4776; c) M. W. Wong, K. B. Wiberg, M. J. Frisch, *J. Am. Chem. Soc.* **1992**, *114*, 523; d) M. W. Wong, K. B. Wiberg, M. J. Frisch, *J. Chem. Phys.* **1991**, *95*, 8991; e) M. W. Wong, K. B. Wiberg, M. J. Frisch, *J. Am. Chem. Soc.* **1992**, *114*, 1645.
[19] M. J. Frisch, G. W. Trucks, H. B. Schlegel, G. E. Scuseria, M. A. Robb, J. R. Cheeseman, J. A. Montgomery Jr, T. Vreven, K. N. Kudin, J. C. Burant, J. M. Millam, S. S. Iyengar, J. Tomasi, V. Barone, B. Mennucci, M. Cossi, G. Scalmani, N. Rega, G. A. Petersson, H. Nakatsuji, M. Hada, M. Ehara, K. Toyota, R. Fukuda, J. Hasegawa, M. Ishida, T. Nakajima, Y. Honda, O. Kitao, H. Nakai, M. Klene, X. Li, J. E. Knox, H. P. Hratchian, J. B. Cross, C. Adamo, J. Jaramillo, R. Gomperts, R. E. Stratmann, O. Yazyev, A. J. Austin, R. Cammi, C. Pomelli, J. W. Ochterski, P. Y. Ayala, K. Morokuma, G. A. Voth, P. Salvador, J. J. Dannenberg, V. G. Zakrzewski, S. Dapprich, A. D. Daniels, M. C. Strain, O. Farkas, D. K. Malick, A. D. Rabuck, K. Raghavachari, J. B. Foresman, J. V. Ortiz, Q. Cui, A. G. Baboul, S. Clifford, J. Cioslowski, B. B. Stefanov, G. Liu, A. Liashenko, P. Piskorz, I. Komaromi, R. L. Martin, D. J. Fox, T. Keith, M. A. Al-Laham, C. Y. Peng, A. Nanayakkara, M. Challacombe, P. M. W. Gill, B. Johnson, W. Chen, M. W. Wong, C. Gonzalez, J. A. Pople, *Gaussian 03*, Revision B.05, Gaussian, Inc., Pittsburgh, PA, USA, **2003**.
[20] a) A. D. Becke, *J. Chem. Phys.* **1993**, *98*, 5648; b) C. Lee, W. Yang, R. G. Par, *Phys. Rev. B37* **1988**, 785.
[21] G. A. Patersson, M. A. Al-Laham, *J. Chem. Phys.* **1991**, *94*, 6081.
[22] P. J. Hay, W. R. Wadt, *J. Chem. Phys.* **1985**, *82*, 299.
[23] a) P. J. Hey, W. R. Wadt, *J. Chem. Phys.* **1985**, *82*, 270; b) W. R. Wadt, P. J. Hey, *J. Chem. Phys.* **1985**, *82*, 284.
[24] C. Peng, Y. Alaya, B. Schlegel, M. J. Frisch, *J. Comput. Chem.* **1996**, *17*, 49.

Received: May 23, 2008
Published Online: October 27, 2008

